Received: 3 December 2019 | Revised: 11 March 2020 | Accepted: 6 April 2020

DOI: 10.1002/chir.23232

SPECIAL ISSUE ARTICLE

WILEY

Testing the vibrational exciton and the local mode models on the instructive cases of dicarvone, dipinocarvone, and dimenthol vibrational circular dichroism spectra

Giuseppe Mazzeo[1] | **Ernesto Santoro**[1] | **Sergio Abbate**[1,2] | **Cristiano Zonta**[3] | **Fabrizio Fabris**[4] | **Giovanna Longhi**[1,2]

[1]Dipartimento di Medicina Molecolare e Traslazionale, Università di Brescia, Brescia, Italy

[2]Research Unit of Brescia, Istituto Nazionale di Ottica (INO), CNR, Brescia, Italy

[3]Dipartimento di Scienze Chimiche, Università degli Studi di Padova, Padova, Italy

[4]Dipartimento di Scienze Molecolari e Nanosistemi, Università Ca' Foscari Venezia, Mestre, Italy

Correspondence
Giovanna Longhi, Dipartimento di Medicina Molecolare e Traslazionale, Università di Brescia, Viale Europa 11, 25123 Brescia, Italy.
Email: giovanna.longhi@unibs.it

Funding information
Fondazione Cariplo, Grant/Award Number: Agrofood Lab Brescia & (BODaI-Lab); Ministero dell'Istruzione, dell'Università e della Ricerca, Grant/Award Number: PRIN 2017 program Project 2017A4XRCA_003

Abstract

The vibrational circular dichroism (VCD) spectra of dicarvone (**1**), dipinocarvone (**2**), and dimenthol (**3**) have been recorded in the range 900–3200 cm^{-1}, encompassing the mid-infrared (mid-IR), the C═O stretching, and the CH-stretching regions. For compound **3** also, the fundamental and the first overtone OH stretching regions have been investigated by IR/NIR absorption and VCD. Density functional theory (DFT) calculations allow one to interpret the IR and VCD spectra and to confirm the configuration/conformational studies previously conducted by X-ray diffraction. The most intense VCD signals are associated with the vibrational normal modes involving symmetry-related groups close to the CC bond connecting covalently the two molecular units. The vibrational exciton (VCDEC) model is fruitfully tested on the VCD data of compounds **1** and **2** for the spectroscopic regions at ~1700 cm^{-1}, and the local mode model is tested on compound **3** at ~3500 and ~6500 cm^{-1}. For compounds **1** and **2** also, ECD spectra are reported, and the exciton mechanism is tested also there, and connections to the VCDEC model are examined.

KEYWORDS

dicarvone, dimenthol, dipinocarvone, ECD, local modes, NIR-VCD, VCD, vibrational excitons

1 | INTRODUCTION

Recently, we measured the vibrational circular dichroism (VCD) spectra of (*endo,endo*)-bicamphor, (*exo,exo*)-bicamphor, and (*exo,endo*)-bicamphor,[1] to check the validity and/or limitations of the vibrational exciton model (which we call here VCDEC=VCD exciton coupling). The VCDEC model had been resumed, with several examples, by Taniguchi and Monde,[2] and was in large part inspired by the successful exciton model for the interpretation of the ECD spectra (ECD = electronic circular dichroism spectra or CD in the UV range); the latter approach was developed by Professor Nakanishi in a large number of papers of which we cite only two representatives.[3,4] The VCDEC model was applied to the case of interacting C═O stretching vibrations but was recognized to work also for other spectroscopic regions and other normal modes[5–7] and had been introduced earlier under the name

Dedicated to Professor Koji Nakanishi.

[This article is part of the Special Issue: In honor and memory of Prof. Koji Nakanishi. See the first articles for this special issue previously published in Volumes 31:12, 32:3, 32:4, 32:5, and 32:6. More special articles will be found in this issue as well as in those to come.]

of coupled dipoles or coupled oscillators.[8–11] The discussion that ensued generated few more contributions, evidencing aspects encountered and investigated since long ago and novel facets regarding the applicability or critical aspects of the model.[12–15] Even though the performance of density functional theory (DFT) is improving from year to year and makes the use of approximate models, like VCDEC, unnecessary for small organic molecules, their use for larger systems, like biopolymers or complex systems presenting through space coupling, is still needed. The VCDEC approach has been adopted among the others by Schweitzer–Stenner et al.[16,17] Alternative approximated methods can be found like fragmentation methods with Hessian reconstruction, which have been applied by Choi and Cho,[18] and in general, intermode coupling between pair of local modes models have been used to calculate the 2D infrared (IR) spectra.[19,20]

The usefulness of the molecular models examined in Abbate et al.[1] relied on two important properties: (i) the C_2 symmetry of tested molecules and (ii) the rigidity of tested molecules, with the conformational mobility confined to just one degree of freedom, namely, the intermolecular dihedral angle. Property (i) makes the VCD spectra to look easily "readable," notwithstanding the high number of vibrational degrees of freedom; whenever we encountered symmetry, VCD spectra looked simple.[1,21,22] Property (ii) allowed us to pinpoint the tiny unbalance of two conformations of opposite interunit dihedral angle, which was also dependent on solvent. In the present work, we treat three further cases: the (*R*,*R*′)-dimer of (*R*)-(−)-carvone (**1**), the (*R*,*R*′)-dimer of (1*R*,5*R*)-(+)-pinocarvone (**2**), and (1S,1′S,2S,2′S,5*R*,5′*R*)-2,2′-diisopropyl-5,5′-dimethylbicyclohexy-1,1-diol, which we will call dimenthol for short, (*S*,*S*′)-**3** or even (**3**) (see Scheme 1, where also the structure for the (−)-pinocarvone (**4**) molecule is presented, which had never been studied before by VCD or ECD).[23,24]

For these molecules, few extra degrees of freedom, besides the interunit dihedral angle, may contribute to conformational mobility and thus may in principle perturb the application of the vibrational exciton model, and one purpose of this work is to enquire to which extent this is taking place.

Indeed, we will investigate to what extent the VCDEC model applies in the C═O stretching spectroscopic region in **1** and **2**. For compound **3**, VCD spectra in the OH stretching fundamental and first overtone regions have been recorded, and the local mode model has been employed to interpret the VCD data.[11,25] The ECD spectra have also been recorded, and a discussion will be presented as to whether the phenomena of vibrational and electronic excitons are related and to which extent.

2 | MATERIALS AND METHODS

2.1 | Materials

The synthesis, characterization, and X-ray structures of compounds **1**, **2**, **3**, and **4** are described in previous works.[23,24] One of the authors of those papers is participating in this work also, and the products are from their collection.

2.2 | VCD and ECD spectroscopies

Absorption and ECD spectra were recorded at room temperature on a JASCO J815SE spectropolarimeter, using 0.1- and 0.2-mm path-length quartz cuvettes for **1** and **2**, respectively, and concentrations of about 1.0×10^{-3} M in chloroform and acetonitrile, as specified in the figure captions. VCD/IR spectra were recorded on a Jasco FVS6000 FTIR spectrometer equipped with a VCD module, comprising a wire-grid linear polarizer, a ZnSe photo elastic modulator to produce 50 kHz modulated circularly polarized radiation over a rather wide range (from 4000 to 850 cm^{-1}), and a liquid N_2-cooled MCT detector; 5000 scans were acquired for each spectrum, and solvents VCD and IR spectra were subtracted. For the OH stretching region and for the CH stretching region, an InSb detector was employed. The spectra were recorded in $CDCl_3/CCl_4$ solutions in 0.2- and 0.1-mm path-length BaF_2 cells with concentrations ranging from 0.05 to 0.1 M. For the OH stretching fundamental region infrasil®/quartz rectangular 0.1- to 0.5-mm-thick cuvettes were employed, on the same Jasco FVS6000 apparatus with solutions as just above. For acquiring NIR-VCD spectra, the home built dispersive apparatus previously used in analogous circumstances was employed,[25–28] a

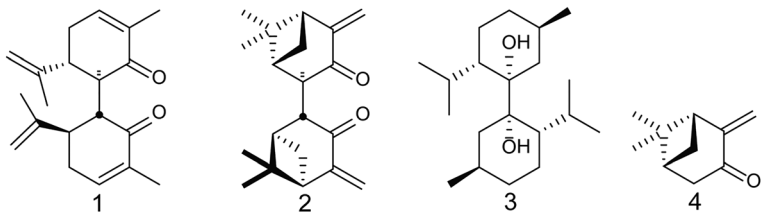

SCHEME 1 Structures of the studied compounds. Configurations: for **1**: (1*R*,2*R*, 1′*R*,2′*R*); for **2**: (1*R*,2*R*,5*R*, 1′*R*,2′*R*,5′*R*); for **3**: (1*S*,2*S*,5*R*,1′*S*,2′*S*,5′*R*); for **4**: (1*R*,5*R*)

suprasil®/quartz cell 0.5 cm wide was employed, and five scans were acquired in the CD and absorption baseline (ABL) mode,[26] the latter being subtracted from the former. The solvent spectrum recorded in the same manner was finally subtracted out. The resolution was 2 nm in the range 1600–1300 nm, with a scan speed of 1 nm/s.

2.3 | DFT calculations

The minimum energy conformers found by MM were further fully optimized by Gaussian16 package,[29] using the DFT at the B3LYP/TZVP level in gas phase (results not shown). DFT allows one to generate IR and VCD spectra from calculated frequencies and dipole and rotational strengths;[30] results were obtained in the IEF-PCM approximation[31] and were plotted by assigning a 4- to 16-cm^{-1} bandwidth Lorentzian band shape to each vibrational transition with a program resident in the Jasco VCD software package. Various scaling factor values were adopted for each compound in different spectroscopic regions and were applied to calculated vibrational transitions. They are specified in the relevant figure captions. To account for mechanical and electrical anharmonicity, as first described in Gangemi et al .,[27] calculations for the overtone/NIR case were conducted for dimenthol **3** and for (*R*)- and (*S*)-menthol and are described in the Section 3.

3 | RESULTS AND DISCUSSION

Let us analyze the three cases separately, beginning with

a Dicarvone (**1**)

In Figure 1, we compare the experimental and the calculated IR and VCD spectra for dicarvone (*R*,*R*)-(**1**). One may notice a pretty good correspondence between experiment and theory, with just the IR bands being calculated slightly too intense with respect to experiments; we do not think this is due to the bandwidth being chosen too narrow in the calculation, since the VCD spectra appear evaluated with correct magnitudes, compared with experiment, with the same choice of bandwidth. The IR spectrum in the CH stretching region does not appear completely well predicted, but this is expected, due to the neglect of anharmonic effects in the present calculations; still, the corresponding VCD spectrum is well accounted for by calculations, with the interpretation commented later on in the paper. The calculated spectra reported in Figure 1 are the weighted averages for three conformers differing mostly in the orientation of the isopropylene group (top part of Figure 2). The IR and VCD spectra for each conformer are given in Figures S1 and S2.

For the main scope of the article, the most interesting spectroscopic region is the C═O stretching region between 1600 and 1700 cm^{-1}, which consists of a single excitonic feature, which is positive and points to a positive dihedral angle between the two C═O bonds. Sure enough, the DFT calculations bear on this point: indeed, three stable geometrical structures are predicted, differing in the dihedral angle defining the position of the isopropylene group about the CC bond connecting it to the carvone ring (see Figure 2), but not on the interunit dihedral angle: the population factors, reported in Figure 2 (top part), allowing to weigh the calculated spectra, are due the product of Boltzmann thermal factors and degeneracy factors associated with either C_2-symmetric or non-symmetric relative positions of the two isopropylene groups. The most populated conformer predicted by DFT is compared with the structure obtained by X-ray[23] in Figure S3: the two structures look quite similar indeed. The interunit dihedral angle ϕ, defined as O═C–C═O (alternatively and equivalently, we can evaluate the interunit dihedral angle as θ = C–C–C–C), does not change much in the three conformers, and O═C–C═O is about +109° for all three conformers **1a**, **1b,** and **1c**, being associated to a P helicity.

In Figure S4 (left), we report the interconversion energy curve between different stable minima obtained by optimizing the structure **1a** for all but one degree of freedom, namely, the C–C–C–C θ torsion. All three structures discussed here are for the minimum of that energy profile at $\theta \approx 70^\circ$, corresponding to $\phi = 109^\circ$; the next minimum along this curve is approximately 5 kcal/mol above the lowest energy minimum, and activation energies are high, above 20 kcal/mol.

In Table 1, we provide calculated frequencies, dipole, and rotational strengths for all three conformers of **1**, according to full DFT calculations and according to the vibrational exciton simplified approach, presented in eqns. 1–3 of Abbate et al .,[1] which we repeat here in the particular case of the C_2 symmetry of the dimeric molecule:

$$\nu_{\pm} = \nu \pm \frac{D}{hc} d^{-3} \left[\sin^2\alpha \cdot \cos\phi + 2\cos^2\alpha\right], \quad (1)$$

$$D_{\pm} = D \pm D\left[\sin^2\alpha \cdot \cos\phi - \cos^2\alpha\right], \quad (2)$$

$$R_{\pm} = \mp \frac{\pi\nu_{\pm}}{2} dD \sin^2\alpha \cdot \sin\phi. \quad (3)$$

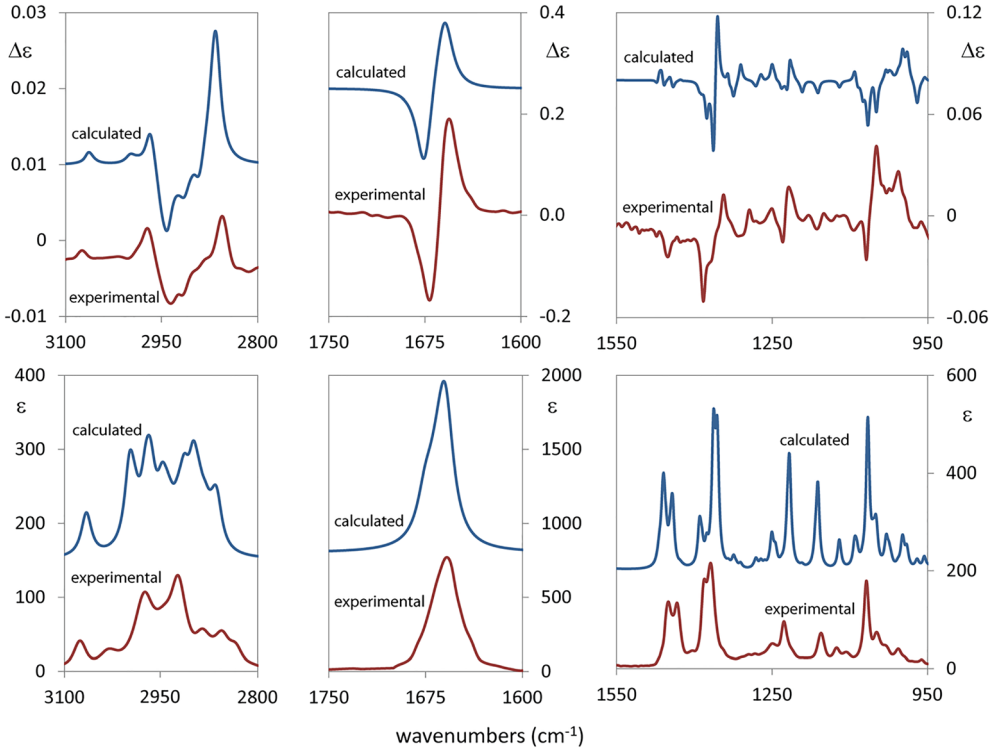

FIGURE 1 Experimental VCD/IR spectra for **1** in solution (chloroform, solid red trace) and computed spectra (B3LYP/TZVP/IEFPCM = chloroform) for **1** (solid blue trace). Scaling factors: 0.955 in the CH stretching region; 0.98 in the C═O/C═C stretching region; 0.98 in the mid-IR region

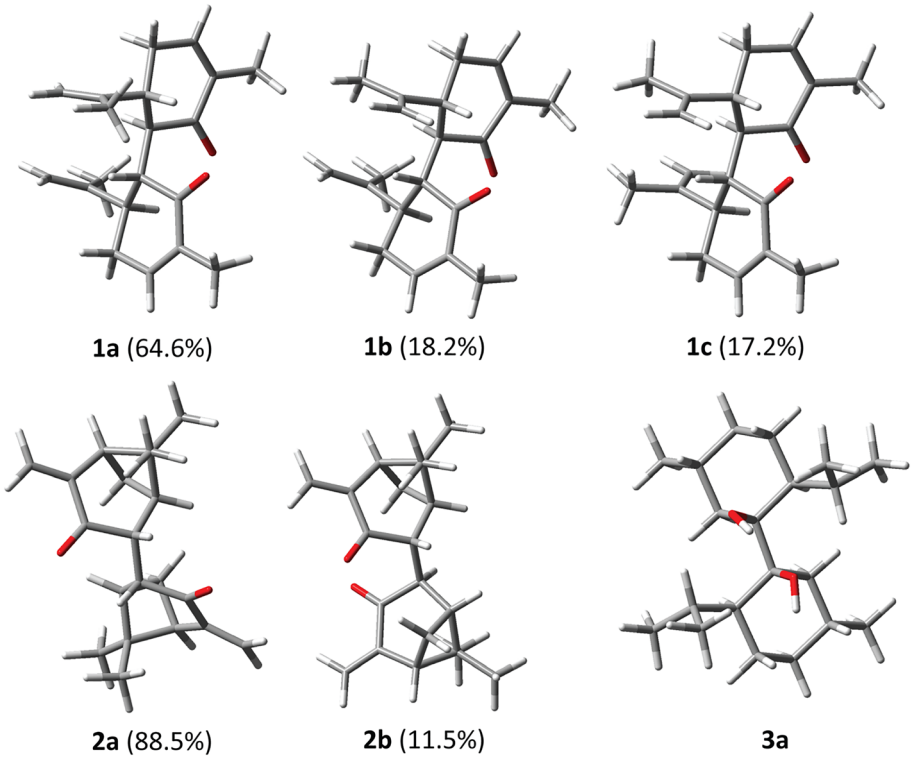

FIGURE 2 Conformers and population factors (B3LYP/TZVP/IEFPCM = $CHCl_3$) of the three conformers of **1** (top line), of the two conformers of **2** (bottom left) and of the single conformer of **3** (bottom right)

In the above equations, the dipole strength D for each isolated C═O normal mode is in esu^{2}cm^2 (as well as the coupled quantities $D_{\pm}$ and $R_{\pm}$), the distance between the oscillators d is in cm, and the frequency ν for the isolated C═O in cm^{-1}, as well as the $\nu_{\pm}$ for the coupled C═O oscillators. In Table 1, one may find also the main

TABLE 1 Geometrical parameters taken into account for the two carbonyl bonds in molecule **1** (B3LYP/TZVP/IEFPCM = $CHCl_3$) and calculated frequencies ($\nu_\pm$), dipole strengths ($D_\pm \times 10^{40}$), and rotational strengths ($R_\pm \times 10^{44}$) for the carbonyl stretching symmetric and antisymmetric couplets, according to full DFT and to vibrational exciton simplified approach (Equations 1, 2, and 3)

Conformers B3LYP/TZVP (IEFPCM = chloroform)									
	1a			**1b**			**1c**		
	DFT	**VCDEC (1)**	**VCDEC (2)**	**DFT**	**VCDEC (1)**	**VCDEC (2)**	**DFT**	**VCDEC (1)**	**VCDEC (2)**
ϕ (°)		109	105		109	105		111	107
d (cm)		3.00E-08	4.26E-08		3.00E-08	4.27E-08		2.95E-08	4.19E-08
α (°)		77.4	67.9		77.2	68.1		77.0	67.3
ν_+ (cm^{-1})	1709.7	1716.6	1721.3	1709.3	1716.7	1721.2	1706.6	1715.9	1721.2
ν_- (cm^{-1})	1693.8	1723.8	1720.5	1693.9	1723.7	1720.6	1692.2	1724.5	1720.6
D_+ (esu^2cm^2)	377.3	571.9	569.6	417.1	571.0	570.7	285.8	535.5	534.3
D_- (esu^2cm^2)	1038.8	1208.7	1211.0	1053.4	1209.6	1209.9	1423.3	1245.1	1246.3
R_+ (esu^2cm^2)	−631.4	−648.2	−851.8	−642.5	−647.2	−856.0	−539.9	−625.0	−819.5
R_- (esu^2cm^2)	398.0	650.9	851.5	449.2	649.9	855.7	810.6	628.1	819.2

Note. Two choices for the electric dipole transition moment (EDTM) origin are made, VCDEC (1) and VCDEC (2) (see text).
Different colors used for providing better readability of data

geometrical characteristics needed for the application of the VCDEC model to the O═C–C═O moiety: $\alpha_1 = \alpha_2 = \alpha$ = C–C═O in-plane angles, ϕ = O═C–C═O dihedral angle, d = CC distance. For the VCDEC calculations, we employed the dipole strength and frequency value for the C═O stretching normal mode, calculated on the most populated conformer of carvone, that is, $D = 890.3 \times 10^{-40}$ esu^2cm^2 and $\nu = 1720.9$ cm^{-1}(vide infra). Equations (1–3), that is, the vibrational exciton simplified approach, assume that magnetic dipole transition moment (MDTM) contributions can be disregarded, an explicative counterexample may be found in Abbate et al.[15] In the case considered here, we have similar VCD intensities for the two components of the doublet (both from experiment and DFT calculations) and a low value for MDTM; these considerations suggest to rely on the simplified model. Two choices for locating the interacting electric dipole transition moments (EDTMs) are proposed and discussed in the following: VCDEC (1) and VCDEC (2). In the first one, VCDEC (1), EDTMs are located on the carbon atoms of the C═O bonds. In the second one, VCDEC (2), the origin of EDTM is at centers of the CC bonds bridging the C═O and the endocyclic C═C (see Figure 3; only one conformer is shown, since the other two do not differ in the d, ϕ, and α parameters, as of Figure 2). The correspondence between the DFT and VCDEC (1) approaches is pretty good for all three conformers for $D_\pm$ and $R_\pm$ but not for $\nu_\pm$, which are inverted in VCDEC (1) calculations with respect to full DFT calculations. This produces the wrong prediction of the VCD C═O stretching couplet. In the following, we analyze what causes the discrepancy. Differences in the

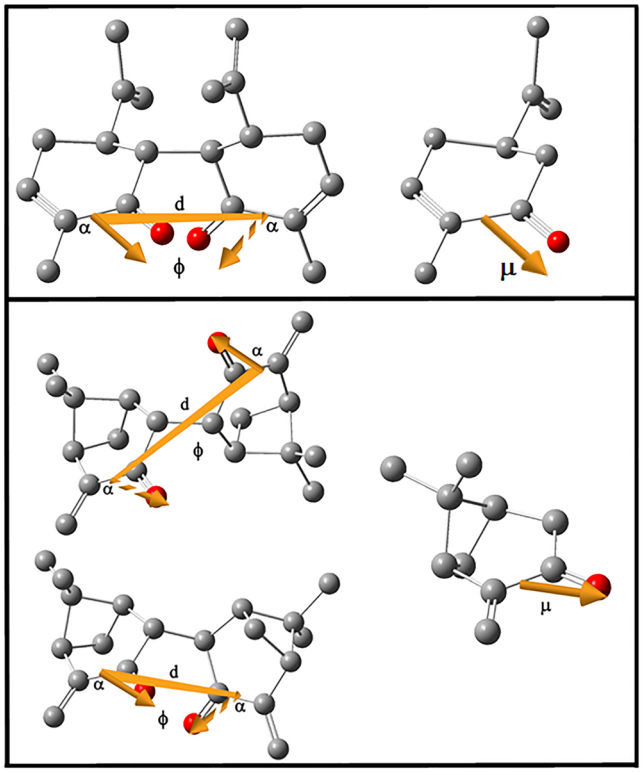

FIGURE 3 Positioning of electric transition dipole moments as in the VCDEC (2) choice for compounds **1** (upper section, one conformer only, since the three conformers are very similar) and **2** (lower section, two different conformers) and for their relative monomer (*R*)-carvone and (1*R*,5R)-(+)-pinocarvone. The values for geometrical parameters ϕ, d, and α_1 and α_2 are given in Table 1 and 2

conformations of the isopropylene units have no influence on the sign and magnitude of the VCD and IR signals in the C═O stretching region (composed of

frequencies, dipole, and rotational strengths); see Figure S2.

The wrong prediction of $\Delta\nu = \nu_+ - \nu_-$ could mean that the separation of ν_+ and ν_- may not be due to dipole coupling only.[12] Looking more closely, we see that this discrepancy in wavenumber is related to the fact that ϕ is larger than 90°, and this should be kept in mind in general: indeed, when this ϕ value, even not changing the P helicity, is slightly higher than 90°, gives a negative value to $\Delta\nu$; the value of α becomes then crucial in determining the predominance of the $\sin 2\alpha \cos\phi$ term in Equation 1. Instead for $\phi < 90°$, $\Delta\nu$ would be positive in any case. In Figure S5, we plot $\Delta\nu$ as functions as of ϕ and α, for limited interval of $\phi > 90°$ and $\phi < 90°$: also, α may be important to decide the ν_+/ν_- order especially for $\phi \approx 90°$ where $\cos\phi \approx 0$. Careful analysis of the normal modes indicates that the C═O stretching mode, bearing the highest EDTM among all vibrational modes, is not completely localized on the carbonyl. Considering carvone, the single exocyclic C═C stretching frequency is calculated as 1701.8 cm^{-1}, while the endocyclic one is at 1690.9 cm^{-1}, with approximately one tenth of the IR intensity of the C═O. In the monomer, the three vibrations are highly localized; instead, the dimer carbonyl stretchings and endocyclic C═C stretchings are highly coupled, but just two modes bear high EDTM, the ones whose characteristics are reported in Table 1.

The delocalized nature of the modes led us to adopt a new origin for EDTM provided in Figure 3 in the center of the simple CC bond connecting the C═O and the endocyclic C═C bond. This generated new d, ϕ, and α geometrical parameters for the VCDEC (2) model and provided a sign reversal for $\Delta\nu = \nu_+ - \nu_-$ giving the correct answer for the coupled oscillators. The interested readers may also consider the approach adopted by Nicu that can reduce whichever normal mode rotational strength to an ad hoc coupled oscillator mechanism, without losing any contribution calculated by DFT.[13,14]

As anticipated above, conformational differences in the isopropylene moieties between the three conformers have modest influence onto calculated IR and VCD spectra, even for the mid-IR region. This may be appreciated in Figures S1 and S2, where the calculated spectra for the three conformers are compared with experiment: only the VCD features at approximately 1250 cm^{-1} have some variability in the three conformers, but the population averaged spectrum allows one to predict quite well experimental data. Even the C–H stretching region shows acceptable correspondence between experiments and calculations, even though the conformers give different answers according to the orientation of the exocyclic group (see Figure S2). For completeness, we measured the IR and VCD spectra of both enantiomers of carvone; results agreed with literature data,[32,33] both from the experimental and theoretical point of view. We provide the results in Figures S6, S7, and S8, together with the DFT calculations, which allow one to see that the mobility of the isopropylene group has a more important effect onto the mid-IR part of VCD and IR spectra than in **1**. In Figure S7, we give the three calculated conformers for carvone.

In Figure 4, we show the ECD experimental and calculated spectra of **1**, which compare quite well. A prominent excitonic-like feature centered at approximately 240 nm (cfr. also the UV band) is appearing, with positive shape: from Table S1 and Figure S9, one may see that the couplet is due to two $\pi \rightarrow \pi^*$ transitions involving the C═O moieties and the C═C endo bonds (and, to lesser extent, also the exo C═C bond orbitals). In a way, this is similar to what happens in VCD; C═O and endocyclic C═C groups constitute the moieties responsible for both the vibrational and electronic excitons.[34] The negative feature observed at approximately 200 nm, quite well predicted, contains two $\pi \rightarrow \sigma^*$ transitions. Finally, a very weak negative broad feature centered at 340 nm is observed and predicted: it has $n \rightarrow \pi^*$ character. The sign of the latter transition is negative and is the same as the sign for the optical rotation provided in Mazzega et al.[23] as if it were the dominant contribution in the Kramers-Kronig transform rule, presented in previous studies.[35,36,37]

b Dipinocarvone (**2**)

In Figure 5, we report the comparison of experimental and calculated IR and VCD spectra in IEF-PCM approximation of dipinocarvone (*R*,*R*)-**2**. In the

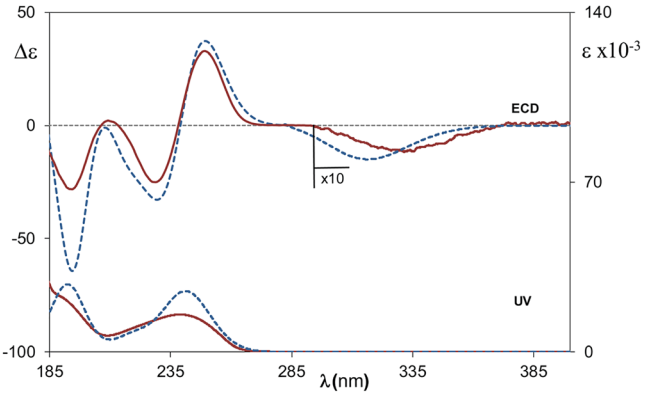

FIGURE 4 Experimental ECD/UV–vis spectra for **1** in solution (acetonitrile, solid red trace) and computed spectra (TDDFT/CAM-B3LYP/aug-cc-pVDZ/IEFPCM = acetonitrile) for **1** (dashed blue trace). (σ = 0.3 eV). A wavelength red shift of 8 nm has been applied. The magnitude of ECD spectra is enhanced from 290 to 380 nm

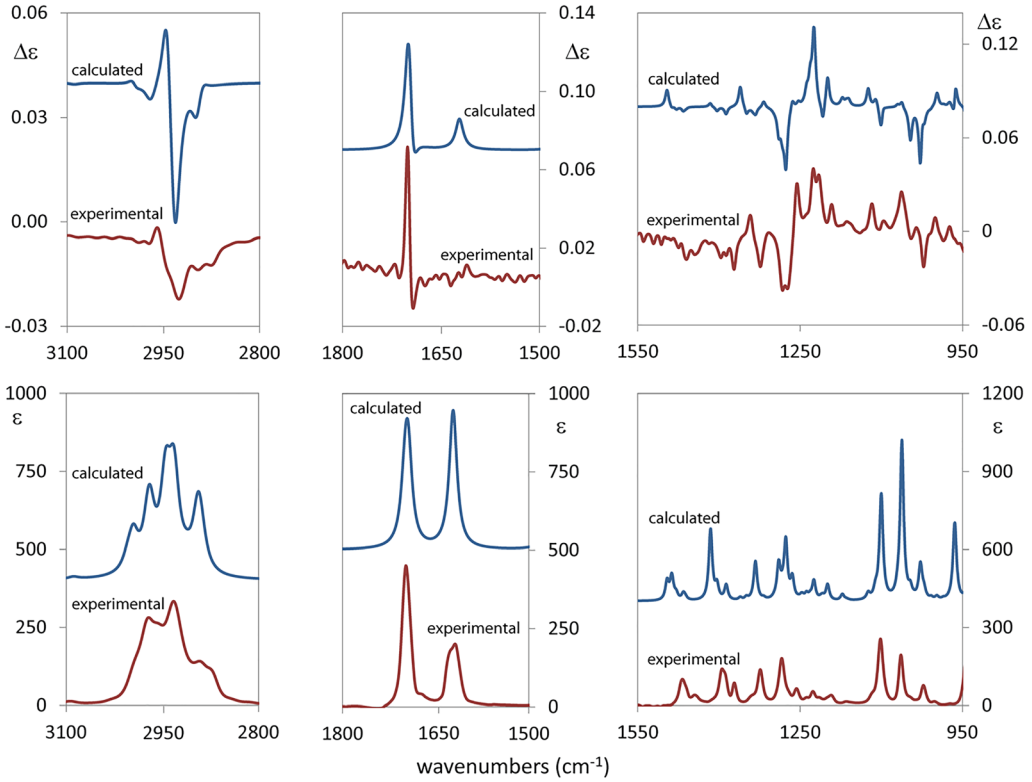

FIGURE 5 Experimental VCD/IR spectra for **2** in solution (chloroform, solid red trace) and computed conformer-averaged spectra (B3LYP/TZVP/IEFPCM = chloroform) for **2** (solid blue trace). Scaling factors: 0.955 in the CH stretching region; 0.97 in the C═O/C═C stretching region; 0.985 in the mid-IR region

Supporting Information, we provide the comparison of experimental IR and VCD spectra for **2** and the corresponding calculated spectra of each one of the two conformers of **2** (Figure S10 for the mid-IR and Figure S11 for the C═O stretching and the CH stretching regions). The comparison is pretty good in all three investigated spectroscopic regions, and the computational performance being similar as in the previous dicarvone case. Indeed, we still notice that the IR intensities are slightly overestimated in the fingerprint region. The VCD spectra are predicted very well.

The populated conformations in this case are just two, as presented in the lower left part of Figure 2. In this case, since the two halves of the molecule are quite rigid, the two predicted conformations, which are populated at approximately 88% and at 12%, correspond to two minima of M and P helicity, respectively, (see Figure S4 and also Figure S3 for comparison with X-ray structures:[23] the M helicity prevails over the P one being the only one observed in the solid state). For completeness, we compare in Figure 6 the experimental and calculated IR and VCD spectra of pinocarvone (**4**);[23] the C═O stretching region is omitted since the VCD signal was too weak to be considered reliable. One may appreciate that in the mid-IR and in the CH stretching region, the observed (and calculated) features of the pinocarvone monomer **4** and dimer **2** are quite similar (in the case of **4**, only one conformer is predicted): the latter spectroscopic region has essentially a broad negative VCD corresponding to a broad structured IR absorption band. The close similarity of the IR and VCD spectra of **2** and **4** leads us to conclude that the normal modes underlying the various bands of these two spectroscopic regions have an intramonomeric nature.

The C═O stretching region is an exception in this respect: the g ratio for the observed positive VCD band of dipinocarvone, (*R*,*R*)-**2**, is approximately 1.6×10^{-4}, which is slightly less than in dicarvone, **1**, (2.5×10^{-4}). Even though the two cases presented here have definitely a smaller g than bicamphors, where g is of the order of 5×10^{-4},[1] yet their g is still fairly big; however, in **2**, the couplet is rather unsymmetrical, with prevailing positive component at higher wavenumbers. The DFT calculations reproduce these data rather well, and the two predicted conformers have M (major conformer **2a**) and P (minor conformer **2b**) helicity, with a partial cancellation of the excitonic aspect and prevalence of M over P (see Figure S11). The results for the approximate VCDEC model, in comparison with results from complete DFT calculation, are given in Table 2, where, besides the

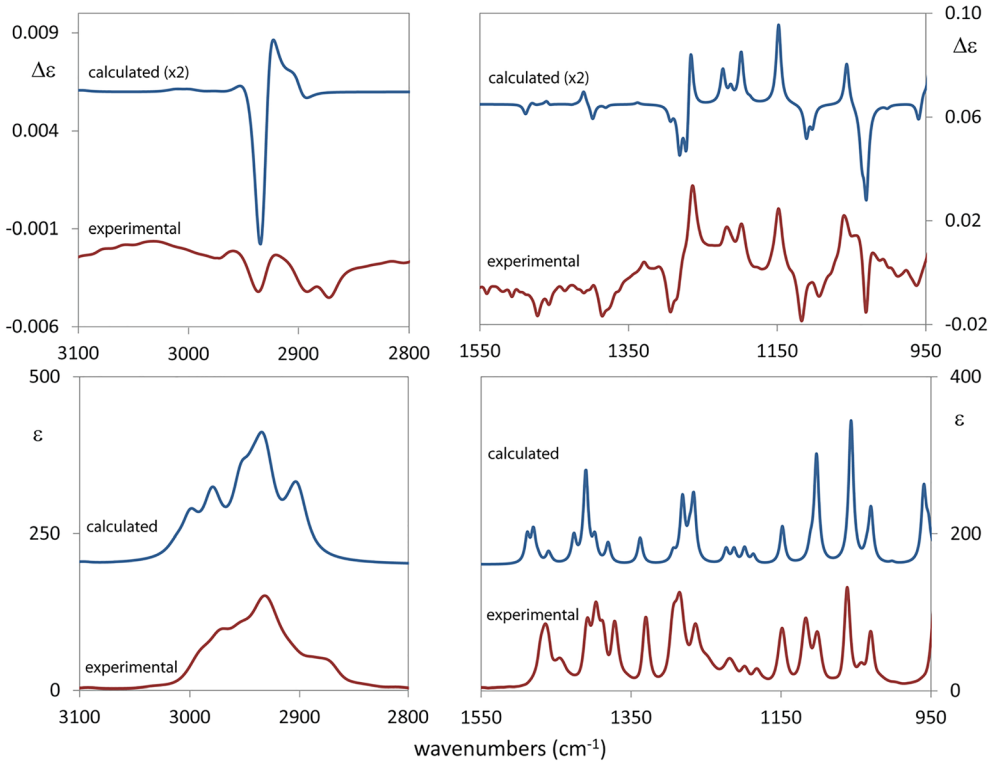

FIGURE 6 Experimental VCD/IR spectra for **4** in solution (tetrachloromethane, solid red trace) and computed spectra (B3LYP/TZVP/IEFPCM = tetrachloromethane) for **4** (solid blue trace). Scaling factors: 0.96 in the CH stretching region; 0.98 in the mid-IR region

TABLE 2 Geometrical parameters taken into account for the two carbonyl bonds in the molecule **2** (B3LYP/TZVP/IEFPCM = $CHCl_3$) and calculated frequencies ($\nu_{\pm}$), dipole strengths ($D_{\pm} \times 10^{40}$), and rotational strengths ($R_{\pm} \times 10^{44}$) for the carbonyl stretching symmetric and antisymmetric couplets, according to full DFT and to vibrational exciton simplified approach VCDEC (Equations 1, 2, and 3)

	Conformers B3LYP/TZVP (IEFPCM = chloroform)					
	2a			**2b**		
	DFT	**VCDEC (1)**	**VCDEC (2)**	**DFT**	**VCDEC (1)**	**VCDEC (2)**
ϕ (°)		−98.6	−96.2		100.6	105.8
d (cm)		3.88E-08	5.04E-08		2.87E-08	3.40E-08
α (°)		99.2	85.8		79.6	61.4
ν_+ (cm^{-1})	1749.6	1759.4	1759.6	1752.7	1758.9	1760.4
ν_- (cm^{-1})	1744.4	1759.9	1759.8	1745.3	1760.5	1759
D_+ (esu^2cm^2)	272.1	290.0	310.8	119.6	276.3	196.2
D_- (esu^2cm^2)	328.7	409.9	389.3	398.2	423.7	503.8
R_+ (esu^2cm^2)	314.3	361.4	482.1	−203.6	−263.8	−287.1
R_- (esu^2cm^2)	−188.6	−361.5	−482.2	264.1	264.0	286.9

*Note.*Two different choices of the EDTM origins are made in VCDEC(1) and VCDEC(2) (see text).

geometric parameters discussed below, we have used the value $\nu = 1759.7$ cm^{-1} and $D = 350.0 \times 10^{-40}$ esu^2cm^2, for the isolated C═O stretching, as obtained from the pinocarvone, **4**, calculations. Again, two choices for locating interacting EDTM are proposed. VCDEC (1) is the usual choice with the origin of EDTM in C of C═O bonds; VCDEC (2) accounts for the delocalization of the 1759.7 cm^{-1} normal mode of the monomer unit, pinocarvone, which can be represented as an antisymmetric C═O/C═C stretching: this suggests to adopt the EDTM

origin at the centers of the CC bonds connecting the two C═O and C═C moieties and a tilted orientation with respect to the C═O bond as derived from the EDTM orientation calculated on the single pinocarvone molecule. (Once again, see also Figure 3 for the VCDEC(2) origins of both conformers of molecule **2**.) The correspondence between the results for ν, D, and R from the two VCDEC models and full DFT presents, for both the M and the P conformers, problems similar to those encountered in dicarvone, suggesting again that positioning of the interacting EDTM is crucial to obtain acceptable results with VCDEC model.

Finally, we report in Figure 7 the UV and ECD experimental and calculated spectra for **2** and **4** close to each other.

In correspondence of the UV feature at approximately 240 nm, one has a positive ECD band for both dipinocarvone and pinocarvone, which witnesses the intramonomer character of this $\pi \rightarrow \pi^*$ transition for the C═C/C═O moiety in this case. The negative ECD feature in dipinocarvone at approximately 210 nm is too far removed from that region, to be considered as the other component of an exciton couplet. It is also worthwhile to notice the inversion of the broad band at 330 nm, which is positive for pinocarvone and negative for dipinocarvone. In the case of **4**, the $n \rightarrow \pi^*$ transition exhibits vibronic feature as reported in literature for other α,β-unsaturated ketones.[34] From Tables S2 and S3 and Figures S12 and S13, one may see that the HOMO → LUMO transition in the two cases is dominating the ECD spectrum at 330 nm, especially for **4**; this transition contains important contributions both from the C═O $n \rightarrow \pi^*$ and from diene π orbitals, so as to make the application of the octant rule inapplicable. This may justify the difference in sign for the ECD band at 330 nm for **2** and **4**. Differently from ECD, VCD brings in some information about mutual orientation of the two pinocarvone moieties.

c Dimenthol (**3**)

The case of dimenthol (**3**) is different from the cases of **1** and **2**, since in **3**, the two OH groups across the bridging CC bond have obviously quite different spectroscopic properties from the C═O groups in **1** and **2**. In Figure 8, for **3** (in the (1*S*,2*S*,5*R*,1*S*′,2*S*′,5*R*′) configuration), we compare the experimental and calculated IR and VCD spectra in the CH stretching and mid-IR spectroscopic regions. The calculated spectra result from just one populated conformer (Figure 2, bottom line), which shows strong similarity with the X-ray structure proposed in Peters et al.[24] (see Figure S3, bottom part). Indeed, even in solution, the menthol ring is in the chair conformation, the hydroxyl groups appear to be held in one conformation by hydrogen bonding interactions, and the isopropyl groups are also in the same conformation as in the solid, due to hydrophobic interactions with other groups in the molecule. In (−)-(1*R*,2*S*,5*R*)-menthol, the OH-rotational degree of freedom has some influence on the isopropyl orientation (Figure S14), while in dimenthol, only one conformer is present: the change in configuration at carbon 1 from (−)-(1*R*,2*S*,5*R*)-menthol to (1*S*,2*S*,5*R*,1*S*′,2*S*′,5*R*′)-dimenthol gives an axial orientation to the two dimenthol hydroxyl groups. The predicted spectra compare quite favorably with the experimental ones; the same happens for (−)-menthol, which possesses five conformers (see Figures S15 and S16 and other

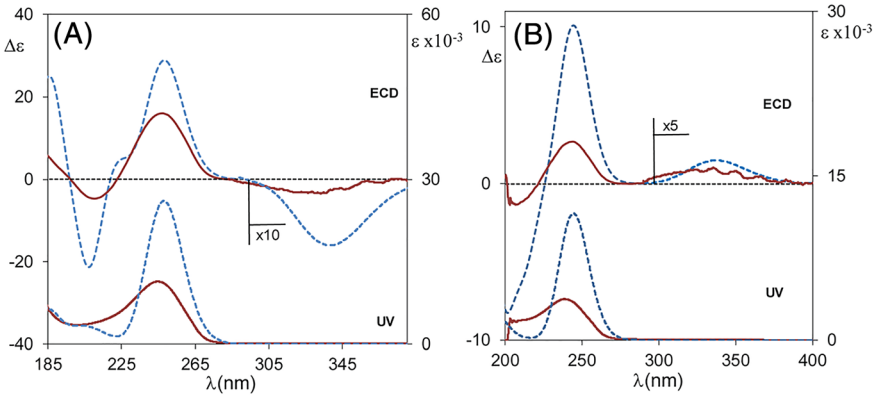

FIGURE 7 A, Experimental ECD/UV–vis spectra of **2** in solution (acetonitrile, solid red trace) and computed spectra (TDDFT/CAM-B3LYP/aug-cc-pVDZ/IEFPCM = acetonitrile) of **2** (dashed blue trace). (σ = 0.3 eV); B, experimental ECD/UV–vis spectra of **4** in solution (Tetrahydrofuran, solid red trace) and computed spectra (TDDFT/CAM-B3LYP/aug-cc-pVDZ/IEFPCM = Tetrahydrofuran) of **4** (dashed blue trace). (σ = 0.3 eV). A wavelength red shift of 8 nm has been applied. For both **2** and **4**, the magnitude of ECD spectra is enhanced from 290 to 400 nm

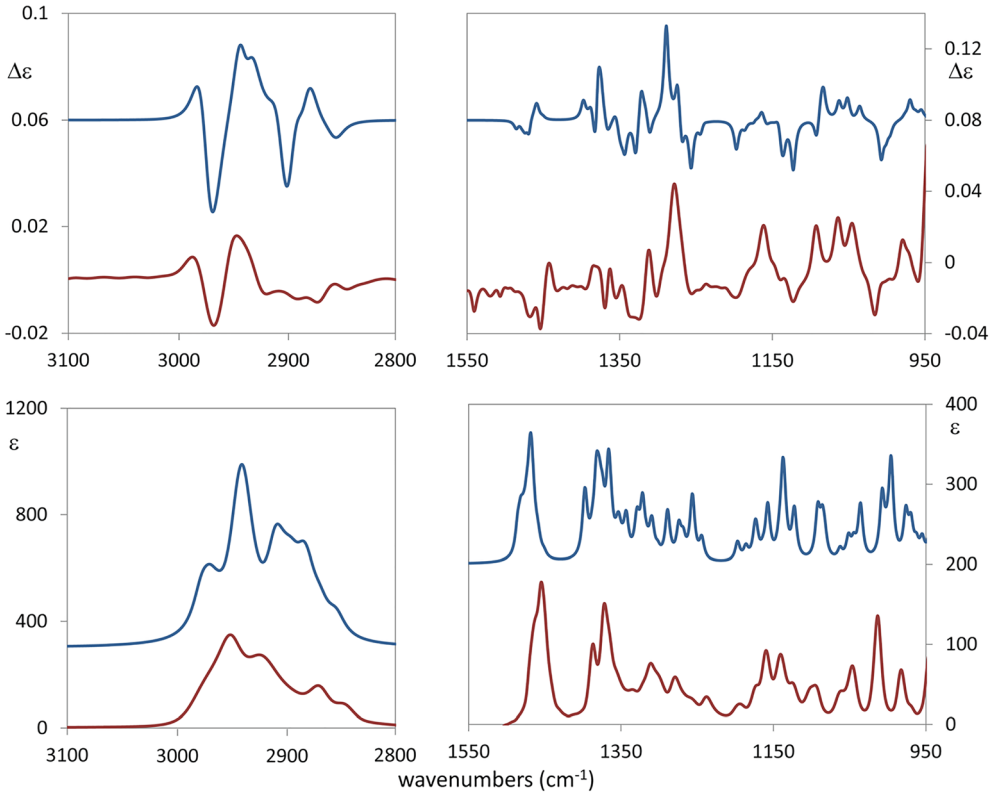

FIGURE 8 Experimental VCD/IR spectra for **3** in solution (carbon-tetrachloride, solid red trace) and computed spectra (B3LYP/TZVP/IEFPCM = carbon-tetrachloride) for **3** (solid blue trace). Left: CH stretching region; right: mid-IR region. Scaling factors: 0.95 in the CH stretching region; 0.98 in the mid-IR region

works[32,33,38] for the mid-IR region and literature[32,39] for the CH stretching region).

A few considerations may be drawn from Figure 8: the IR spectrum is well predicted by DFT calculations in band position and intensity, the latter aspect being treated better in **3** than for **1** and **2**. The VCD band at approximately 1260 cm^{-1} is positive for dimenthol and negative for (−)-menthol. This is indeed somewhat expected, since the latter compound has opposite configuration at carbon 1 (AC: (1*R*,2S,5*R*)) with respect to dimenthol (AC: (1*S*,2*S*,5*R*,1*S*′,2*S*′,5*R*′)), and at that frequency, one has normal modes possessing C*H-bending character, as noticed also, for example, in Abbate et al. and Mazzeo et al.[40–42] We checked that the most important contribution is from the C*H-bending at 1,1′ while C*H-bending at 2,2′ (with the same configuration in (−)-menthol and dimenthol) and C*H-bending in the isopropyl group contribute to a lesser extent to that band. Differences in the IR and VCD spectra of (−)-menthol and dimenthol are also noticed in the 1150–1050 cm^{-1} region, but they are not as clear-cut as for the band at approximately 1260 cm^{-1}.

Also, the CH stretching region brings in interesting information: in (−)-(1*R*,2*S*,5*R*)-menthol, one has a characteristic triplet of VCD bands at 2945, 2928, and 2911 cm^{-1} with alternating signs (+, −, +) and a broad (−) VCD band, affected by anharmonicity at 2870 cm^{-1}. In (1*S*,2*S*,5*R*,1*S*′,2*S*′,5*R*′)-dimenthol, one still has a VCD triplet at 2985, 2965, and 2945 cm^{-1} with the signs (+, −, +) (shifted upwards with respect to (−)-menthol) and with the broad (−) VCD band extending from 2960 to 2920 cm^{-1}. Following Gangemi et al.[11] and Laux et al .,[39] we checked that the characteristic VCD triplet originates from CH_2-antisymmetric normal modes coupled to a C*H stretching mode located in the CH_2–CH_2–C*H fragment at positions 3, 4, and 5, which have the same configuration in monomer and dimer.

Finally, we investigated the fundamental and first overtone OH stretching regions. Reference can be made to our previous, experimental and theoretical studies[25–28,43] and to the experimental and computational study by Devlin et al .,[44] as well as, limited to absorption, to the seminal overtone investigations of alcohol and diol OH stretchings.[45,46] In Figure 9, we compare the experimental IR/NIR absorption and VCD spectra in the OH stretching fundamental (Δv = 1) and first overtone (Δv = 2) regions of (1*S*,2*S*,5*R*,1*S*′,2*S*′,5*R*′)-dimenthol and of (+)-(1*S*,2*R*,5*S*)- and (−)-(1*R*,2*S*,5*R*)-menthol, with the corresponding calculated spectra of (1*S*,2*S*,5*R*,1*S*′,2*S*′,5*R*′)-dimenthol and of (1*R*,2*S*,5*R*)-

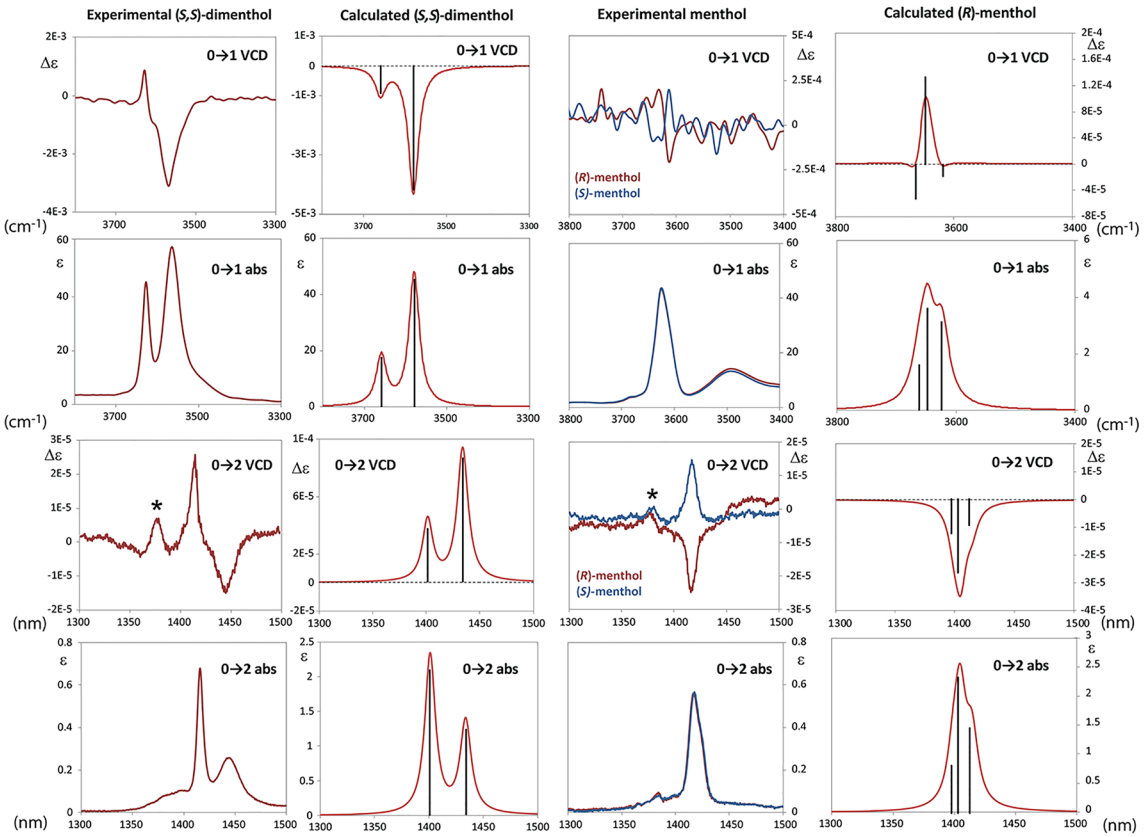

FIGURE 9 Comparison of experimental (first and third columns) and calculated (second and fourth column) (on the basis of the local mode model) absorption and VCD spectra in the OH stretching transitions $\Delta v = 1$ and $\Delta v = 2$ of (1*S*,2*S*,5*R*,1*S*′,2*S*′,5*R*′)-dimenthol (first two columns) and of (−)-(1*R*,2*S*,5*R*)-menthol (last two columns); the experimental VCD spectra of menthol for also the (+)-enantiomer are superposed to the ones of the (−)-enantiomer (the positive VCD band marked (*) observed at 1370 nm is an anomaly due to the gratings)

menthol, according to the local mode approximation.[25–28] This approximation for IR-VCD and NIR-VCD spectra has been discussed in previous studies[25–28] and implies the calculations of mechanical and electrical anharmonicities. Application of the local mode model to the present case of two nearby OH bond stretchings is to be taken with some care, even though, according to Kjaergaard[45] and Abbate et al .,[47] is expected to work increasingly better with increasing overtone order. Once calculated the mechanical harmonic frequency ω and anharmonicity χ of the local OH oscillators, we compute frequencies $\nu_{0-1} = \omega\text{-}2\chi$ and $\nu_{0-2} = \omega\text{-}6\chi$; after evaluation of the necessary electrical anharmonic terms, we calculated also dipole strengths D_{0-1} and D_{0-2} and rotational strengths R_{0-1} and R_{0-2} for $\Delta v = 1$ and $\Delta v = 2$ transitions, for the single OH local oscillator of (1*R*,2*S*,5*R*)-menthol and for the two supposedly decoupled OH bond stretchings of (1*S*,2*S*,5*R*,1*S*′,2*S*′,5*R*′)-dimenthol. These parameters are reported in Table 3, and in Figure S17, we report $APT_{iz}(H)$ and $AAT_{iz}(H)$, i = x,y,z.

We first notice that the experimental VCD spectra of dimenthol are quite intense both in the fundamental and in the first overtone region, and also the g ratios (g = (Δε/ε)) are high; for menthol, VCD signals are weaker. In detail, in the case of menthol, one absorption band and one VCD band are recorded for $\Delta v = 2$, while for $\Delta v = 1$, two very weak VCD features are recorded at the same frequency of the absorption band at about 3600 cm^{-1} (the second absorption band at $\Delta v = 1$ is due to intermolecular hydrogen bonded species, but we ignore it in the present study). Instead, for dimenthol, two absorption bands are recorded, and they are largely independent of concentration (ranging from 0.0125 to 0.2 M; see Figure S18). According to the results of Table 3, they are due to acceptor (high frequency) and donor (low frequency) OH stretching local modes. We notice that the linear and nonlinear electric and mechanical characteristics of the acceptor OH bond are more similar to the corresponding ones of menthol than the donor's, especially considering the menthol conformer for HOCH dihedral ≈ 174°.

The predicted absorption spectra compare well with the experimental ones both for (*R*)-menthol and for (*S*,*S*)-dimenthol, in shape and frequency; intensities for $\Delta v = 1$ for menthol are underestimated, while intensities for $\Delta v = 2$ are overestimated for both molecules. A

TABLE 3 Top: population factors, calculated dihedral angle (HOCH for menthol and HOCC for dimenthol), ϖ (OH) stretching frequencies calculated with Gaussian at the harmonic level (B3LYP/TZVP), mechanical frequency ω (OH), and anharmonicity parameter χ (OH) of the single OH bond in three conformers of (*R*)-menthol (see Supporting Information) and of the two OH bonds in (*S*,*S*)-dimenthol calculated by energy fit along the local coordinate.[26,27] Bottom: first two columns, APTzz(H) ($\partial\mu z/\partial z$) element and its derivative ($\partial^2\mu z/\partial z^2$) with respect to z (z-axis along the OH bond), dipole *D* and rotational strengths *R* for the 0 → 1 and 0 → 2 transitions for the single OH bond in (*R*)-menthol in three conformations and for the two OH bonds in (*S*,*S*)-dimenthol

	%pop	dihedral (°)	ϖ (OH) (cm^{-1})		ω (OH) (cm^{-1})	χ (OH) (cm^{-1})
(−)-Menthol						
Conformer 1	37	64.4	3808		3825	88.6
Conformer 2	34.5	174.4	3786		3802	89.2
Conformer 3	17.8	−53.5	3822		3838	88.4
(S,S)-Dimenthol						
Donor OH	100	38.8	3747		3762	91.6
Acceptor OH	100	160.6	3822		3838	89.9
	$\partial\mu z/\partial z$ (H) (e)	$\partial^2\mu z/\partial z^2$ (H) (e/Å)	*D* (0–1) (10^{-40} esu^2cm^2)	*D* (0–2) (10^{-40} esu^2cm^2)	*R* (0–1) (10^{-44} esu^2cm^2)	*R* (0–2) (10^{-44} esu^2cm^2)
(−)-Menthol						
Conformer 1	0.101	−0.573	9.75(19.00)	6.02	1.15(3.86)	−0.22
Conformer 2	0.093	−0.393	9.06(15.94)	4.05	−0.25(−0.57)	−0.07
Conformer 3	0.093	−0.504	8.76(15.88)	4.87	−1.02(−5.74)	−0.18
(S,S)-Dimenthol						
Donor OH	0.198	0.041	57.61(54.1)	1.65	−13.03(−26.00)	0.29
Acceptor OH	0.125	−0.282	21.04(23.70)	2.79	−2.75(−2.66)	0.13

Note. The values reported in parenthesis are obtained by standard DFT calculations in the harmonic approximation. For complete information about the necessary electrical parameters, see Figure S18.

first good result of the local mode approach is that we calculate frequencies quite close to experimental values, without using ad hoc scaling factors, and we obtain overtone intensities of the correct order of magnitude. Dipole and rotational strengths obtained by standard DFT harmonic calculations for the fundamental transitions compare well with the ones obtained by the anharmonic local mode approach: the anharmonic contribution to 0–1 intensity is weak; besides, we have noticed that normal modes associated with OH stretchings in dimenthol actually are localized on each bond. For VCD bands, the prediction for $\Delta v = 1$ is good for the main feature of dimenthol, while the high frequency/low intensity feature is not accounted for in sign both by the local mode approach and by DFT harmonic calculations.

For $\Delta v = 2$, the observed single feature of menthol is well predicted in sign and intensity, while for dimenthol, only the acceptor high frequency band is well predicted, whereas the broad band attributed to the donor is predicted with the wrong sign. Further analysis of these discrepancies is needed in a future work.

4 | CONCLUSION

In this work, we have investigated by VCD spectroscopy three compounds having two identical interacting units with limited conformational mobility with the aim to test approximate models often used in the literature to elucidate their limitations in order to apply them more reliably: the models are the vibrational exciton (VCDEC) model and the anharmonic local mode model. The former is used to study the carbonyl stretching region of compounds **1**, dicarvone, and **2**, dipinocarvone, the latter model is used to study the hydroxyl stretching region in the fundamental and first overtone range of compound **3**, dimenthol. For sake of completeness also mid-IR VCD spectra and ECD spectra are presented and interpreted.

For dicarvone, **1**, the measured couplet in the C═O stretching region is clear, strong, positive, and is easily associated to P helicity (with interbond dihedral angle equal to +109°) and predicted by full DFT calculations; however, it is not predicted in frequency by the VCDEC model when interacting dipoles are placed on the C═O bonds. The observation that C═O stretching modes

couple with nearby C═C stretching modes led us to displace the origin of the interacting dipoles towards the C═C, obtaining thus the correct result. Similar considerations have been applied to **2**, dipinocarvone; the observed weak and asymmetric negative couplet in the C═O stretching region, which is associated to M helicity and is predicted by full DFT calculations, is also predicted by the VCDEC model if the coupled dipole transition moments are placed in correspondence of the moieties (C═O and C═C) involved in the normal mode. These two examples show how critical is the choice of the origin of coupled dipoles particularly as regards the calculation of the frequency order of the doublet, a problem often disregarded since most of the times attention is paid to the helicity sense of dipoles in the prediction of rotational strength signs. These examples teach us that careful analysis of the normal modes is needed, in order to correctly apply the model to cases different from the standard isolated carbonyls[1,2] or from aromatic moieties[5,6,15]; of course, a precondition is that normal mode transitions have high dipole strength values. Another particularly relevant point of the VCDEC model that we have elucidated here is the choice of the EDTM origin; this has a consequence on the distance of interacting EDTMs and on the value of the other geometrical parameters. The latter aspect has also been discussed by Covington et al.[12] and Nicu[14] and can be important also considering the excitonic model used for electronic CD.[7] As a conclusion of this part of the paper, we are confident that the VCDEC examples provided here help to apply correctly the exciton model, whenever DFT calculations are hard or impossible to perform, due to large molecular dimensionality, like, for example, in the case of biopolymers.[16–20] The presented examples may serve as a warning that making predictions for small molecules by blind application of the VCDEC model can be quite dangerous.

Having a similar goal of testing limitations and applicability of simplified models, we have applied the local mode anharmonic model for the OH stretching fundamental and first overtone IR/NIR VCD spectra of **3** dimenthol. Good results are obtained for frequencies and absorption intensities; VCD features are only partially predicted also considering fundamentals where the normal mode and local mode treatment gives in this case comparable results. Recently,[48] another pair of diols has been investigated by VCD in the fundamental and first overtone OH stretching regions: for the diol in this study and for the two previous ones, the signs of the two OH stretching bands correlate with the absolute configuration of the carbon atoms bearing the hydroxyl groups. Also, in Paoloni et al .,[48] the local mode approach was applied with better correspondence with experimental data.

ACKNOWLEDGMENTS

We gratefully acknowledge financial support from Cariplo Foundation, through Agrofood Lab for ES. Research was carried out with the support of resources of Big&Open Data Innovation Laboratory (BODaI-Lab), University of Brescia, granted by Fondazione Cariplo and Regione Lombardia and of Computing Center CINECA (Bologna), Italy. Finally, we thank MIUR (Italian Ministry of Education, University and Research) for funding under the auspices of PRIN 2017 program: (Project 2017A4XRCA_003 "Physico-chemical Heuristic Approaches: Nanoscale Theory of Molecular Spectroscopy (PHANTOMS)").

ORCID

Sergio Abbate https://orcid.org/0000-0001-9359-1214
Cristiano Zonta https://orcid.org/0000-0003-1749-7482
Giovanna Longhi https://orcid.org/0000-0002-0011-5946

REFERENCES

1. Abbate S, Mazzeo G, Meneghini S, Longhi G, Boiadjiev SE, Lightner DA. Bicamphor: a prototypic molecular system to investigate vibrational excitons. *J Phys Chem A*. 2015;119(18):4261-4267.
2. Taniguchi T, Monde K. The exciton chirality method in vibrational circular dichroism. *J Am Chem Soc*. 2012;134(8):3695-3698.
3. Harada N, Nakanishi K. The exciton chirality method and its application to configurational and conformational studies of natural products. *Acc Chem Res*. 1972;5:257-263.
4. Berova N, Nakanishi K. Exciton chirality method: principles and applications. In: Nakanishi K, Berova N, Woody RW, eds. *Circular Dichroism: Principles and Applications*. New York: Wiley-VCH Publishers; 2000, Chapter 12:337-382.
5. Mazzeo G, Fusè M, Longhi G, et al. Vibrational circular dichroism and chiroptical properties of chiral Ir(III) luminescent complexes. *Dalton Trans*. 2016;45(3):992-999.
6. Mazzeo G, Abbate S, Longhi G, Castiglioni E, Boiadjiev SE, Lightner DA. pH dependent chiroptical properties of (1*R*,2R)- and (1*S*,2*S*)-*trans*-cyclohexane diesters and diamides from VCD, ECD, and CPL spectroscopy. *J Phys Chem B*. 2016;120(9):2380-2387.
7. Szymkowiak J, Kwit M. Electronic and vibrational exciton coupling in oxidized trianglimines. *Chirality*. 2018;30(2):117-130.
8. Su CN, Keiderling TA. Conformation of dimethyl tartrate in solution. Vibrational circular dichroism results. *J Am Chem Soc*. 1980;102:511-515.
9. Nafie LA. *Vibrational Optical Activity, Principles and Applications*. New York: John Wiley and Sons; 2011 (see Appendix 1).
10. Holzwarth G, Chabay I. Optical activity of vibrational transitions: a coupled oscillator model. *J Chem Phys*. 1972;57:1632-1635.
11. Gangemi R, Longhi G, Lebon F, Abbate S, Laux L. Vibrational Excitons in CH-stretching fundamental and overtone vibrational circular dichroism spectra. *Monatshefte Chem*. 2005;136/3:325-345.

12. Covington CL, Nicu VP, Polavarapu PL. Determination of the absolute configurations using exciton chirality method for vibrational circular dichroism: right answers for the wrong reasons? *J Phys Chem A*. 2015;119(42):10589-10601.
13. Nicu VP. Revisiting an old concept: the coupled oscillator model for VCD. Part 1: the generalised coupled oscillator mechanism and its intrinsic connection to the strength of VCD signals. *Phys Chem Chem Phys*. 2016;18(31):21202-21212.
14. Nicu VP. Revisiting an old concept: the coupled oscillator model for VCD. Part 2: implications of the generalised coupled oscillator mechanism for the VCD robustness concept. *Phys Chem Chem Phys*. 2016;18(31):21213-21225.
15. Abbate S, Bruhn T, Pescitelli G, Longhi G. Vibrational optical activity of BODIPY dimers: the role of magnetic−electric coupling in vibrational excitons. *J Phys Chem A*. 2017;121(1): 394-400.
16. Schweitzer-Stenner R, Measey TJ. Simulation of IR, Raman and VCD amide I band profiles of self-assembled peptides. *Spectroscopy*. 2010;24:25-36.
17. Hongen T, Taniguchi T, Nomura S, Kadokawa J, Monde K. In depth study on solution-state structure of poly (lactic acid) by vibrational circular dichroism. *Macromolecules*. 2014;47: 5313-5319.
18. Choi JH, Cho M. Calculations of intermode coupling constants and simulations of amide I, II, and III Vibrational Spectra of Dipeptides. *Chem Phys*. 2009;361:168-175.
19. Buchanan EG, James WH, Choi SH, et al. Single-conformation infrared spectra of model peptides in the amide I and amide II regions: experiment-based determination of local mode frequencies and inter-mode coupling. *J Chem Phys*. 2012;137. 094301
20. Reppert M, Tokmakoff A. Computational amide I 2D IR spectroscopy as a probe of protein structure and dynamics. *Annu Rev Phys Chem*. 2016;67:359-386.
21. Passarello M, Abbate S, Longhi G, Lepri S, Ruzziconi R, Nicu VP. Importance of C*−H based modes and large amplitude motion: effects in vibrational circular Dichroism spectra: the case of the chiral adduct of dimethyl Fumarate and Anthracene. *J Phys Chem A*. 2014;118(24):4339-4350.
22. Abbate S, Ciogli A, Fioravanti S, et al. Solving the puzzling absolute configuration determination of a flexible molecule by vibrational and electronic circular Dichroism spectroscopies and DFT calculations: the case study of a chiral 2,2-Dinitro-2,2-biaziridine. *Eur J Org Chem*. 2010;6193-6199.
23. Mazzega M, Fabris F, Cossu S, De Lucchi O, Lucchini V, Valle G. Synthesis, Atropoisomerism and chemistry of the dimers of *R*-(−)-Carvone, *R*-(−)-Hydrocarvone, 1*R*,5*R*-(+)-Pinocarvone and other Monoterpenic ketones. *Tetrahedron*. 1999;55:4427-4440.
24. Peters K, Peters E-M, Leoni L, Fabris F, De Lucchi O. Crystal structure of (1*S*,1'*S*,2*S*,2'*S*,5*R*,5'R)-2,2′-diisopropyl-5,5′-dimethylbicyclohexy-1,1-diol, $[(CH_3)C_6H_8OH(C_3H_7)]_2$. *Z Kristallogr NCS*. 1999;214:355-356.
25. Abbate S, Longhi G, Castiglioni E. Near-infrared vibrational circular dichroism: Nir-Vcd. In: Berova Polavarapu PL, Nakanishi K, Woody RW, eds. Vol 1, Cap 10, pag 247*Comprehensive Chiroptical Spectroscopy, Volume 1: Instrumentation, Methodologies, and Theoretical Simulations*. 1st ed. NY: John Wiley & Sons, Inc.; 2012.
26. Abbate S, Castiglioni E, Gangemi F, Gangemi R, Longhi G. NIR-VCD, vibrational circular dichroism in the near-infrared: experiments, theory and calculations. *Chirality*. 2009;21: S242-S252.
27. Gangemi F, Gangemi R, Longhi G, Abbate S. Experimental and ab-initio calculated VCD spectra of the first OH-stretching overtone of (1*R*)-(−) and (1*S*)-(+)-*endo*-borneol. *Phys Chem Chem Phys*. 2009;11(15):2683-2689.
28. Castiglioni E, Lebon F, Longhi G, Abbate S. Vibrational circular Dichroism in the near infrared: instrumental developments and applications. *Enantiomer*. 2002;7(4-5):161-173.
29. Frisch MJ, Trucks GW, Schlegel HB, et al. *Gaussian 16*. Wallingford CT: Gaussian, Inc.; 2016.
30. Stephens PJ. The theory of vibrational circular dichroism. *J Phys Chem*. 1985;89:748-752.
31. Tomasi J, Mennucci B, Cammi R. Quantum mechanical continuum solvation models. *Chem Rev*. 2005;105(8):2999-3093.
32. Guo C, Shah RD, Dukor RK, Freedman TB, Cao X, Nafie LA. Fourier transform vibrational circular dichroism from 800 to 10,000 cm^{-1}: Near-IR-VCD spectral standards for terpenes and related molecules. *Vibr Spectrosc*. 2006;42:254-272.
33. Avilés Moreno JR, Partal Ureña F, López González JJ. Conformational landscape in chiral terpenes from vibrational spectroscopy and quantum chemical calculations: *S*-(+)-carvone. *Vibr Spectrosc*. 2009;51:318-325.
34. Lightner DA, Gurst JE. *Organic Conformational Analysis and Stereochemistry from Circular Dichroism Spectroscopy*. John Wiley and Sons Ltd; 2000:487.
35. Moscowitz A. Theoretical aspects of optical activity. Part one: small molecules. In: Prigogine I, ed. Vol. IV *Advances in Chemical Physics*. New York: Accademic Press; 1962:67-112.
36. Giorgio E, Viglione RG, Zanasi R, Rosini C. Ab initio calculation of optical rotatory dispersion (ORD) curves: a simple and reliable approach to the assignment of the molecular absolute configuration. *J Am Chem Soc*. 2004;126(40):12968-12976.
37. Polavarapu PL, Petrovic AG, Zhang P. Kramers-Kronig transformation of experimental electronic circular Dichroism: application to the Analysis of optical rotatory dispersion in dimethyl-L-tartrate. *Chirality*. 2006;18(9):723-732.
38. Avilés Moreno JR, Partal Ureña F, López González JJ. Hydrogen bonding network in a chiral alcohol: (1*R*,2*S*,5*R*)-(−)-menthol. Conformational preference studied by IR–Raman–VCD spectroscopies and quantum chemical calculations. *Struct Chem*. 2013;24:671-680.
39. Laux L, Pultz VM, Abbate S, et al. Inherently dissymmetric chromophores and vibrational circular dichroism. The CH_2-CH_2-C*H fragment. *J Am Chem Soc*. 1982;104:4278-4280.
40. Abbate S, Burgi LF, Castiglioni E, et al. Assessment of configurational and conformational properties of Naringenin by vibrational circular dichroism. *Chirality*. 2009;21(4):436-441.
41. Mazzeo G, Longhi G, Abbate S, Buonerba F, Ruzziconi R. Chiroptical signatures of planar and central chirality in [2]Paracyclo[2](5,8)quinolinophane derivatives. *Eur J Org Chem*. 2014;7353-7363.
42. Gabrieli S, Mazzeo G, Longhi G, Abbate S, Benincori T. Discrimination of axial and central stereogenic elements in chiral Bis (oxazolines) based on Atropisomeric 3,3′-Bithiophene scaffolds through chiroptical spectroscopies. *Chirality*. 2016;28 (10):686-695.

43. Abbate S, Mazzeo G, Longhi G. NIR-absorption and NIR-VCD spectroscopy can teach us a lot about OH bonds. Rendiconti Accademia Nazionale delle Scienze detta dei XL-Memorie di Scienze Fisiche e Naturali 136°, 2018, Vol. XLII, Parte II, Tomo II, pp. 73–80.
44. Devlin FJ, Stephens PJ, Besse P. Conformational rigidification via derivatization facilitates the determination of absolute configuration using chiroptical spectroscopy: a case study of the chiral alcohol endo-borneol. *J Org Chem*. 2005; 70(8):2980–2993
45. Kjaergaard HG, Howard DL. Overtone spectroscopy: a sensitive probe of hydrogen bonding. *Chem New Zealand*. 2006;16-19.
46. Péron J-J, Sandorfy C. The anharmonicity of the OH stretching vibration of hydrogen bonded methanol in binary systems. *J Chem Phys*. 1976;65:3153-3157.
47. Abbate S, Gangemi R, Longhi G. Dipole and rotational strengths for overtone transitions of a C_2-symmetry HCCH molecular fragment using Van Vleck perturbation theory. *J Chem Phys*. 2002;117:7575-7586.
48. Paoloni L, Mazzeo G, Longhi G, et al. Toward fully unsupervised Anharmonic computations complementing experiment for robust and reliable assignment and interpretation of IR and VCD spectra from mid-IR to NIR: the case of 2,3-Butanediol and trans-1,2-Cyclohexanediol. *J Phys Chem A*. 2020;124:1011–1024.

SUPPORTING INFORMATION

Additional supporting information may be found online in the Supporting Information section at the end of this article.

How to cite this article: Mazzeo G, Santoro E, Abbate S, Zonta C, Fabris F, Longhi G. Testing the vibrational exciton and the local mode models on the instructive cases of dicarvone, dipinocarvone, and dimenthol vibrational circular dichroism spectra. *Chirality*. 2020;32:907–921. https://doi.org/10.1002/chir.23232